Integration of Satellite and Surface Data Using a Radiative–Convective Oceanic Boundary-Layer Model

ALAN K. BETTS
Middlebury, Vermont

PATRICK MINNIS
Atmospheric Sciences Division, NASA Langley Research Center, Hampton, Virginia

W. RIDGWAY
Applied Research Corporation, Landover, Maryland

DAVID F. YOUNG
Lockheed Engineering and Sciences Company, Hampton, Virginia

(Manuscript received 27 May 1991, in final form 11 September 1991)

ABSTRACT

A mixing-line boundary-layer model is used to retrieve cloud-top height from satellite-derived cloud-top temperatures, using 700-hPa National Meteorological Center (NMC) analyses and the Comprehensive Ocean and Atmosphere Data Set (COADS) surface data as supporting datasets. Results are compared with the fixed-lapse-rate method of retrieving boundary-layer depth from sea surface temperatures (SST) and cloud-top temperatures. A radiative–convective equilibrium boundary-layer model is used to retrieve boundary-layer structure given SST and surface wind, satellite cloud-top temperatures and cloud fraction, and the 700-hPa NMC thermodynamic analyses. Good agreement is found between the COADS data and the model solutions for low-level temperature and moisture. This suggests that equilibrium boundary-layer models may be of use over remote oceans in the retrieval of boundary-layer structure.

1. Introduction

The convective boundary layer (CBL) plays an important role in controlling the surface fluxes over the ocean, where conventional observations are sparse. Sea surface temperature is routinely retrieved from a combination of ship and satellite data (Reynolds 1988). Cloud-top temperature and cloud fraction can also be retrieved from satellites (e.g., Minnis and Harrison 1984). However, the current satellite atmospheric sounding systems cannot resolve the detailed temperature and moisture structure through the CBL, which is typically only 100–200 hPa deep. In this paper, we address first the retrieval of CBL top height from satellite-derived cloud-top temperature using simple models for the CBL. We then use a one-dimensional radiative–convective model for the CBL to derive the boundary-layer thermodynamic structure given CBL top and cloud fraction. We have also used the National Meteorological Center (NMC) gridded analyses and the marine observations from the COADS (Comprehensive Ocean and Atmosphere Data Set; see Woodruff et al. 1987). These are monthly mean averages of ship observations of SST, deck-level pressure, temperature, humidity, and wind. These are archived in 2° × 2° latitude–longitude bins, and they were interpolated to 2.5° × 2.5° averages to match the resolution of the satellite data. Figures 1 and 2 show the 5-yr mean July SSTs and surface wind streamlines for the northeastern Pacific. These show the characteristic mean gradient of SST from the coast toward the south and southwest along the northeasterly trades on the southeastern side of the subtropical high.

The cloud data used here consist of monthly mean cloud fractions and cloud-top temperatures for low, medium, and high clouds derived from 8-km visible and infrared radiances taken every 3 h by the GOES (Geostationary Operational Environmental Satellite) during July 1983–87. The data were analyzed with the hybrid bispectral threshold method of Minnis et al. (1987) on a 2.5° latitude–longitude grid covering the area between 10°–40°N and 115°–145°W. Only low-level clouds, those with tops below about 2000 m, are

Corresponding author address: Dr. Alan K. Betts, RD#2, Box 3300, Middlebury, VT 05753.

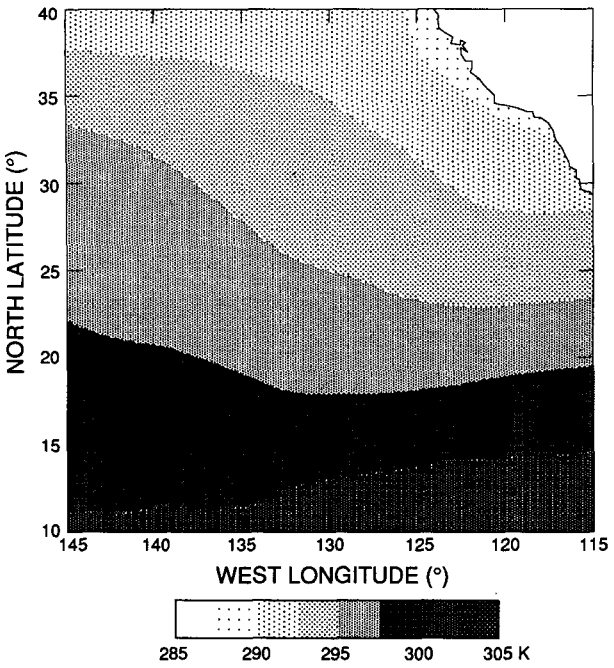

FIG. 1. July mean COADS sea surface temperature (1983–87).

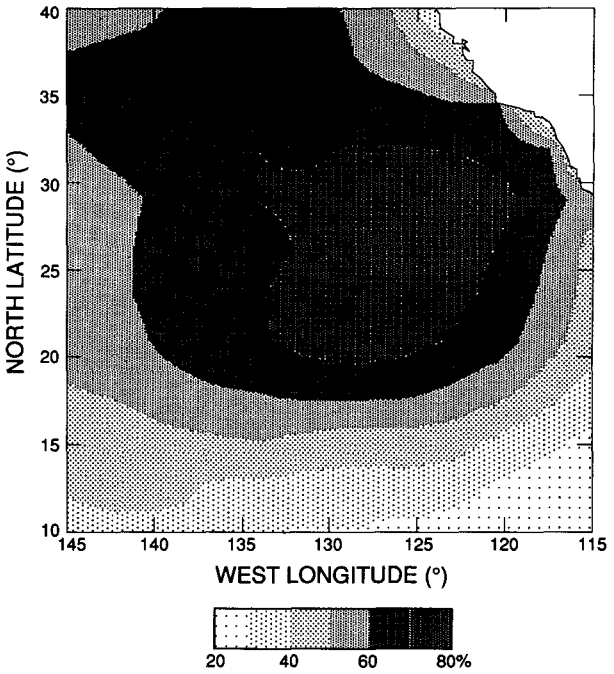

FIG. 3. Mean July low cloud cover from GOES (1983–87; from Heck et al. 1990).

considered here. More details of the analyses are given by Heck et al. (1990). The mean low-cloud amount and the corresponding cloud-top temperatures for the 5-yr period are presented in Figs. 3 and 4, respectively. Mean low-cloud amounts range from less than 30% near the northern California coast to a maximum of ~80% near 25°N, 126°W. Low cloud amounts drop rapidly south of 20°N and gradually west of the maximum. The patterns of cloudiness are consistent with both surface (e.g., COADS) and other satellite analyses (e.g., Sadler et al. 1976). Cloud amounts in Fig. 3 are

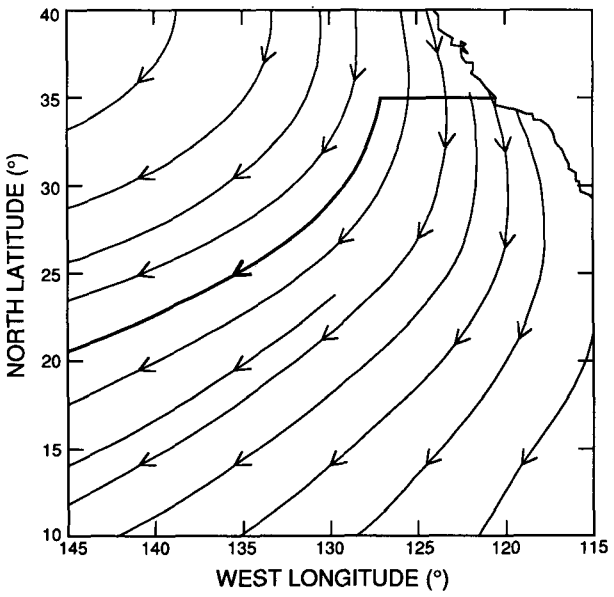

FIG. 2. July mean surface wind streamlines from NMC gridded analyses (1983–87).

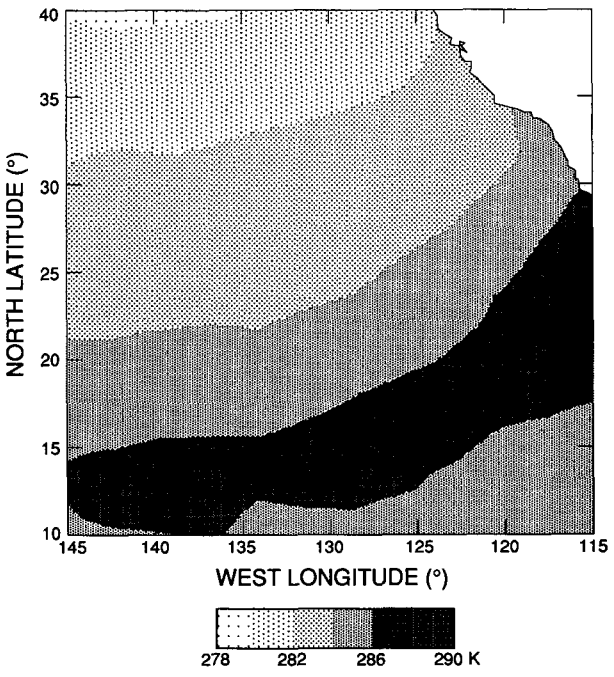

FIG. 4. Mean low cloud-top temperature from GOES (1983–87; from Heck et al. 1990).

slightly less than the former and slightly greater than the latter. The cloud-top temperatures of low clouds in Fig. 4 vary from ≈280 K in the north to about 286 K in a band in the southeast.

2. Retrieval of boundary-layer cloud height

a. *Constant-lapse-rate method*

Minnis et al. (1992) use a mean lapse rate of 7.1 K km^{-1} between the sea surface temperature T_{SST} and the cloud-top temperature, T_{CLD}, to derive cloud-top height. Figure 5 shows the mean cloud-top heights derived from the COADS SSTs from Fig. 1 and low cloud-top temperatures T_{CLD} from Fig. 4 using (1):

$$Z_T = (T_{SST} - T_{CLD})/7.1. \quad (1)$$

Equation (1) represents a simple boundary-layer (BL) "model" with constant mean lapse rate, derived by Minnis et al. (1992) from FIRE sounding data close to the southern California coast. It has only one parameter, but whether it is generally applicable over the oceans is unknown.

b. *Mixing-line method*

In shallow nonprecipitating CBLs, total water q^* and certain combinations of thermodynamic variables, namely, the liquid water or saturation potential temperature θ^* (Betts 1973) and the equivalent potential temperature θ_e^* (Lilly 1968), are conserved to good approximation in both dry- and moist-adiabatic processes and in isobaric mixing processes. If the convective mixing is sufficiently rapid, as it typically is below cloud base, then a nearly well-mixed subcloud layer results: this has long been the basis of mixed-layer representations of the CBL (Lilly 1968; Betts 1973; Tennekes 1973; Stull 1973). The CBL as a whole is typically not well mixed above cloud base, but it is thermodynamically coupled, and the conserved variables follow a nearly linear mixing-line profile for which $(\delta\theta^*/\delta q^*)_{ML} \approx$ constant, as air at different pressure levels in the CBL represents statistically changing mixtures of air from near the surface and the air entrained at CBL top (Betts 1982). Betts (1985) suggested a parametric representation of the CBL based on this mixing-line model, shown schematically on a tephigram in Fig. 6. The lines of constant potential temperature (θ and θ^*) run diagonally and are labeled across the top left-hand corner. The lines of constant mixing ratio are the light dashed lines. The heavy dashed line BC is a mixing line (a line with $\delta\theta^*/\delta q^*$ constant) between cloud base and inversion top. The point B is (θ^*, q^*) of air at cloud base at its lifting condensation level (LCL). The point C is the LCL point for air at the inversion top: the construction is shown by the dotted lines of constant θ^*, q^* (which in this case are just θ, q for unsaturated air). Note that although the inversion top is at p = 810 hPa, to reach saturation, air at this level must be lifted to a *saturation pressure* level p^* = 670 hPa. Just as C is the *saturation point* for inversion top air, the mixing line BC can be thought of as a line joining the saturation points of all mixtures of air with the saturation points B and C (Betts 1982).

Below cloud base there is a second short line AB of constant virtual potential temperature θ_v, representing the weak increase of potential temperature θ and decrease of q at neutral density, which is observed in the subcloud layer over the ocean (e.g., Betts and Albrecht 1987). These mixing lines AB and BC link the properties of air near the surface to the air sinking through the inversion. In this idealization, all the air in the CBL is presumed to have thermodynamic properties lying on these two mixing lines.

In particular, the temperature at the cloud boundary at cloud top T_{CT} lies on the mixing line as shown (see Betts 1982), because air at the cloud boundary is just saturated at that pressure: that is, it has $p = p^*$. We identify this temperature with the satellite radiative temperature of cloud top T_{CLD};

$$T_{CT} = T_{CLD}. \quad (2)$$

We then have cloud-top pressure, provided we have sufficient information to construct the mixing line BC between cloud base and inversion top. This requires a great deal more information than the method in section 2a, where a mean lapse rate was specified, but the method may be more generally applicable.

The detailed profiles of temperature and liquid water

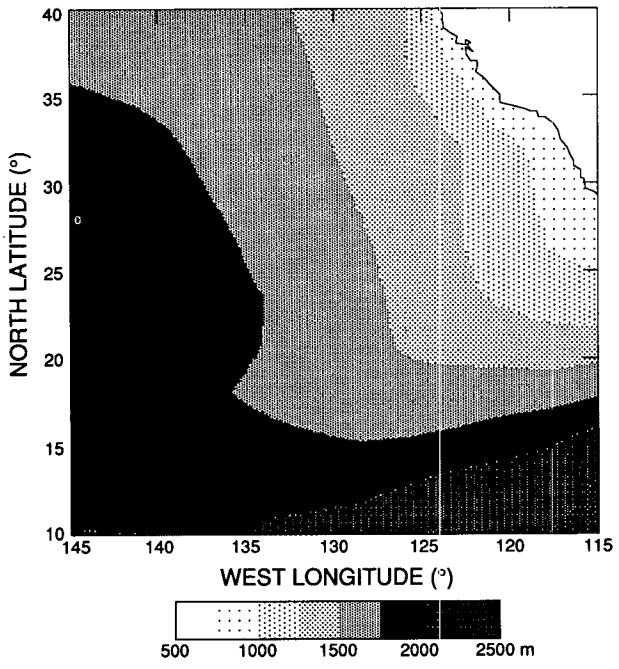

FIG. 5. Mean July low cloud-top heights from GOES (1983–87) using fixed lapse rate of 7.1 K km^{-1}.

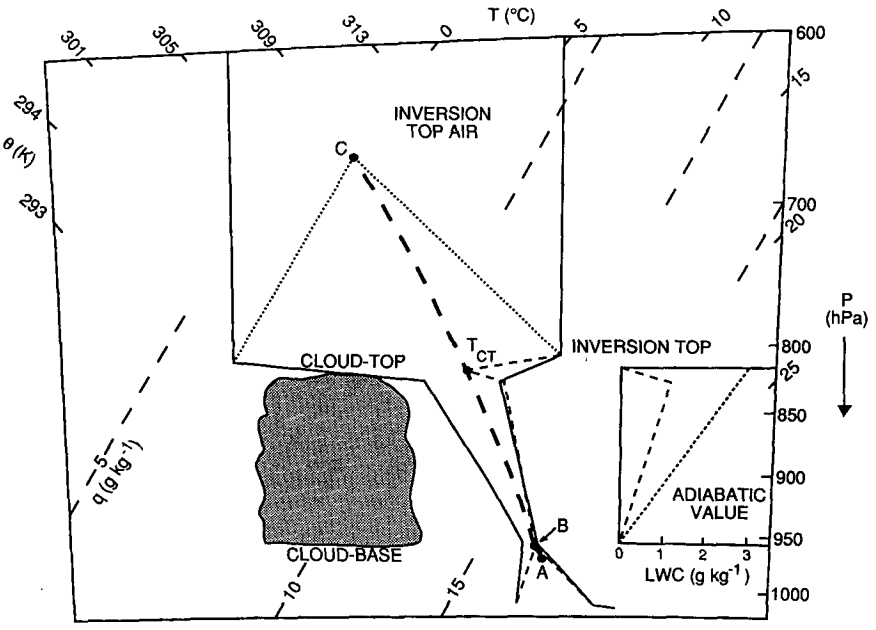

FIG. 6. Tephigram showing profiles of model equilibrium solution for SST = 300.1 K. The clear-air temperature and mixing ratio lines are solid, the in-cloud and below-cloud profiles are short dashed, with liquid water as an inset. The heavy dashed lines *AB* and *BC* are the mixing lines through the subcloud and cloud layers, respectively.

through the CBL, which are also shown in Fig. 6, will be needed later for radiative computations, which will be discussed in section 3. These profiles are determined by specifying different profiles for a parameter

$$\beta = dp^*/dp, \tag{3}$$

the change of saturation level p^* with pressure along the mixing line (Betts 1985). A small value of $\beta = 0.2$ is used to derive point B from A in Fig. 6, consistent with observations in marine boundary layers (Betts and Albrecht 1987).

c. *Boundary conditions above the CBL*

Point C (Fig. 6) above the CBL is needed to determine mixing-line slope. The NMC analyses is used, although these data have serious deficiencies over the northeastern Pacific, where there is little upper-air sounding data. In the absence of observations, the analysis fields depend on initialization and insertion of data from short-term forecasts of the model and in some cases the insertion of bogus humidity data (Timchalk 1986). In addition, changes in the model structure and physics result in changes in the model climatology (see Trenberth and Olson 1988). The 850-hPa analysis-level data is partly inside the model CBL and has generally unrealistically high mixing ratios. There are also serious discrepancies between the low-level NMC data and the COADS data in some years (see next section). Therefore, the NMC 700-hPa data were extrapolated down to point C to determine upper boundary conditions. This was done by assuming constant saturation equivalent potential temperature θ_{es} and constant q from 700 hPa down to the BL top. The use of the NMC 700-hPa analyses with this extrapolation is a deficiency in our analysis. In the tropics, there is typically a decrease of θ_{es} with height in the Pacific above the CBL and often reversals in the water vapor structure (Kloessel and Albrecht 1989). The inadequacy of the NMC data highlights the data problems over the oceans. (One purpose of this study is to suggest that CBL models might be used interactively to improve the satellite retrieval of the BL thermodynamic profiles). Only a 5-yr July average is presented because the variations in the NMC data between years are open to question. Figure 7 shows the NMC mean 700-hPa θ_{es} field for five Julys (1983–87). To the southeast of the high pressure it is relatively flat with $\theta_{es} \approx 351$ K, consistent in the tropical region of the eastern Pacific with Kloessel and Albrecht (1989) and the 1987 FIRE sounding data (Schubert et al. 1987), which show $\theta_{es} \approx 355 \pm 16$ K at the (lower) 850-hPa level. To the northwest, θ_{es} falls at higher latitudes. Figure 8 shows the corresponding NMC 700-hPa mean q field. This is relatively flat near 3 g kg^{-1}, with higher values in the deep tropics. This is again generally consistent with the FIRE sounding data, which show 3.9 ± 2.1 g kg^{-1} at 850 hPa. In the deep tropics, the values of $q \approx 6$ g kg^{-1} are consistent with the Kloessel and Albrecht (1989) study.

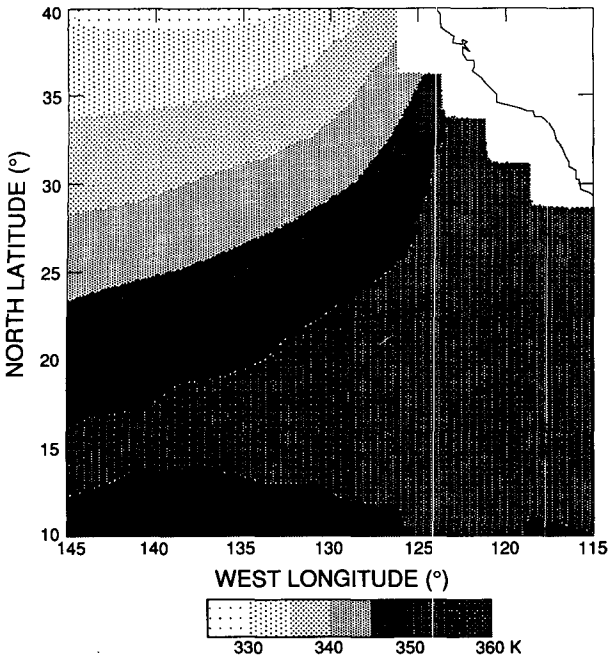

FIG. 7. Mean 700-hPa NMC analysis of saturation equivalent potential temperature θ_{es}.

d. Lower boundary conditions

The constant-lapse-rate method uses SST as a lower boundary condition. The mixing-line method needs atmospheric thermodynamic properties above the ocean surface in the subcloud layer (e.g., the point A in Fig. 6) or near cloud base (point B in Fig. 6). The NMC analysis at 1000 hPa could not be used because there are major inconsistencies from year to year (presumably associated with model changes) and the analyzed data show major errors when compared with the COADS data, which are internally consistent from year to year. For example, in the COADS data the sea–air difference of potential temperature is realistic: it is slightly negative over cold water and increases to a positive value of nearly 1 K at tropical temperatures. However, mean θ at 1000 hPa in the NMC analysis ranges from 1 to 3 K warmer than the corresponding COADS deck-level θ, so that the mean sea–air θ difference is unrealistically negative over the whole domain. Part of this appears to be a model deficiency and part erroneously high SSTs in the NMC analysis in 1986 and 1987. The NMC 1000-hPa mixing ratios are also too high in comparison with the COADS data over the whole domain. Consequently, COADS is used as a lower boundary condition to develop a mixing-line retrieval method for BL depth. In section 3, we shall explore using an equilibrium BL model as a technique to give subcloud layer (θ, q), where none is available.

Deck-level (θ_A, q_A) were used as near surface conditions to define point A in Fig. 6. These were extrapolated to B along a line of constant θ_v using $\beta = 0.2$ in (3). The mixing line BC was then computed using the 700-hPa NMC data to give θ_{es} and q at C, and the cloud-top pressure was found corresponding to T_{CT} on BC.

e. Mixing-line retrieval of cloud top

Figure 9 shows the retrieved cloud-top height field. The pattern is similar to Fig. 5, except derived cloud-top heights are generally 100–150 m lower, except in the northwest where they are $\approx$100 m higher. Figure 10 shows the field of the mean lapse rate between the SST and T_{CT}. Near the California coast and at northern latitudes, the mean lapse rate is around 7 K km^{-1}, corresponding to the fixed value (from Heck et al. 1990) used in deriving Fig. 5. Over much of this domain, however, the mixing-line retrieval gives a mean BL lapse rate of around 7.8 $\pm$ 0.4 K km^{-1}, which gives correspondingly lower BL heights. We conclude that the simple method proposed by Minnis et al. (1992) is an excellent first approximation, but the mean lapse rate over the open ocean may vary by $\pm$15% from their value. In the tropics a better mean value for the BL mean lapse rate would be 7.8 K km^{-1}. Given adequate data, the mixing-line retrieval can improve on Heck et al. (1990) by internally computing this mean lapse rate, as in Fig. 10.

f. Sensitivity studies

The sensitivity to the upper boundary condition is not large, which is fortunate considering the inade-

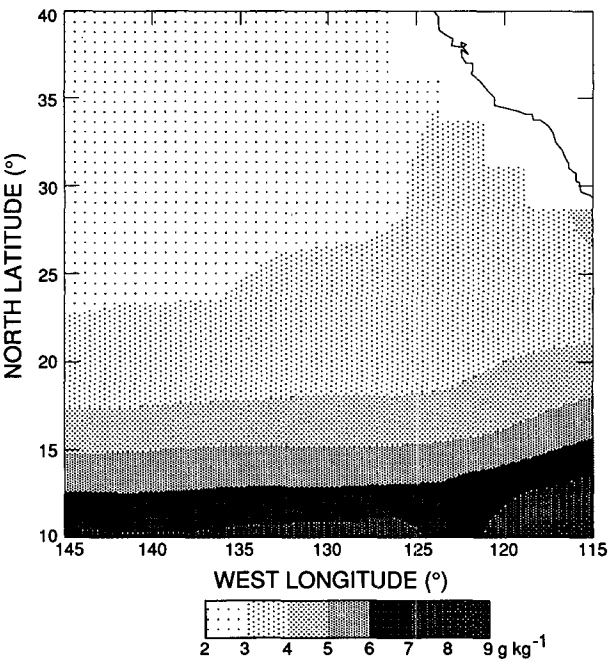

FIG. 8. As Fig. 7 for 700-hPa mixing ratio.

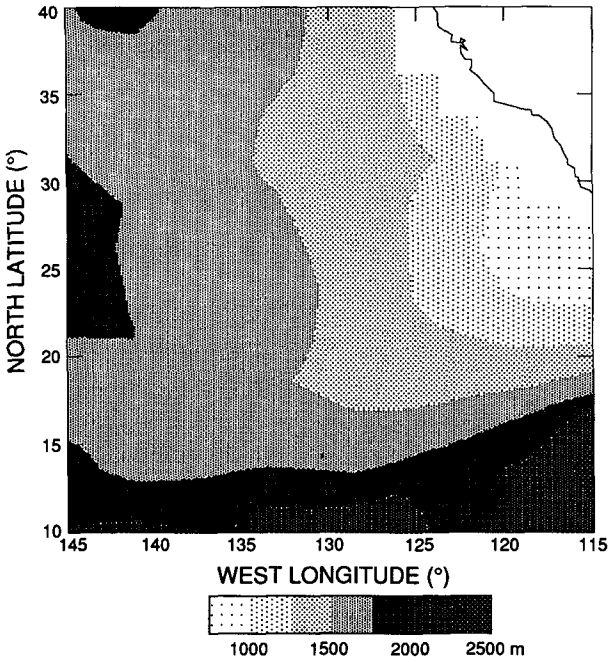

FIG. 9. Mean low cloud-top heights from GOES retrieved using mixing-line retrieval method.

quacies of the NMC analyses. Any change in either upper or lower boundary conditions that moves the mixing line toward higher temperatures increases cloud-top height. Increasing θ_{es} at BL top by 5 K, or increasing cloud-top mixing ratio by 1 g kg^{-1}, increases cloud-top height by about 40 m (slightly more at warm SSTs). The mean NMC analyses could be in error by this amount. At the lower boundary, an increase of θ_A by 1 K or an increase of mixing ratio by 1 g kg^{-1} increases cloud-top height by about 70 m (somewhat less at warm SSTs). The mean COADS data probably have smaller errors than these, since they are derived from the average of many individual temperature and wet-bulb temperature measurements on ships. Some small systematic biases due to ship effects may still be present, however.

3. Use of equilibrium BL model to determine thermodynamic structure

The previous section showed how BL models could be used to estimate BL depth from cloud-top temperature. The simplest model used a fixed lapse rate from the SST. The mixing-line model needs more information: θ and q above the BL and in the subcloud layer. Of these two, it is harder to remotely measure subcloud-layer properties remotely. However, the coupling between SST and subcloud (θ, q) is quite strong over the ocean, so other methods of estimating subcloud-layer properties may be useful. In this section, we discuss the use of a one-dimensional equilibrium radiative–convective boundary-layer model from Betts and Ridgway (1989) to determine the internal structure of the BL over the oceans, and in particular the subcloud θ and q. The reader is referred to this paper for full details of the model. The form in which the model will be used is with specified surface conditions (SST, surface pressure, and wind speed, which will be taken from the COADS), specified cloud fraction (from the satellite data), and specified upper boundary conditions above the CBL (for which NMC data will be used). The model then uses the same mixing-line model shown in Fig. 6 as a parameterization of the BL internal structure and uses a radiation code to compute longwave and shortwave radiative cooling and warming for distinct atmospheric layers, here the subcloud layer and the CBL. Heat and moisture budget equations for these atmospheric layers, together with bulk aerodynamic equations for the surface heat and moisture fluxes, are solved iteratively to find equilibrium solutions for the CBL thermodynamic structure and depth. The model gives equilibrium BL depth and cloud-top temperature as a function of a subsidence parameter at the BL top. The subsidence at BL top is not known, so it was treated as a variable and adjusted to give the observed cloud-top temperature (increasing the subsidence gives a shallower equilibrium BL). These diagnostically determined subsidence values were comparable to the radiative equilibrium subsidence rates found in Betts and Ridgway (1988, 1989). As a test of the usefulness of the model solutions, the model low-level θ and q were then compared with the deck-level COADS data.

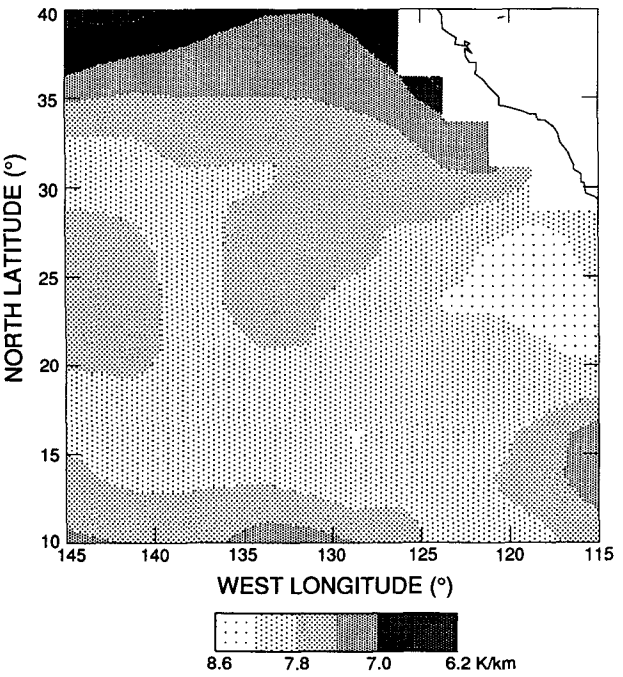

FIG. 10. Mean CBL lapse rate from surface to cloud top from mixing-line retrieval.

a. Mixing-line model profiles

In section 2, the mixing-line model was used to couple near-surface atmospheric properties with cloud-top temperature (which lies on the cloud layer mixing line) and with properties above the CBL. The primary use there was to determine cloud-top pressure from cloud-top temperature. In the radiative equilibrium model, clear and cloudy thermodynamic profiles through the whole CBL are used by the radiation code. The mixing-line model is used to give idealized vertical profiles of temperature, humidity, and liquid water (in clouds) through the CBL and the cloud-top inversion, using different bulk parameters to represent clouds and the clear regions in between them. Figure 6 shows profiles on a thermodynamic diagram for the model solution with SST = 300.1 K. The clear-air temperature and mixing ratio are the solid lines; the profiles below and in cloud are shown with short dashes. The model is a slight extension of Betts and Ridgway (1989) in that the subcloud-layer thermodynamic profiles follow a dry virtual adiabat (constant θ_v from A to B), as discussed in section 2b. In effect, we have two distinct mixing lines: one following a dry virtual adiabat below cloud base, where the change in conserved variables with pressure is small, and then a second mixing line from cloud base through the cloud layer (heavy dashes from B to C), linked to the properties of the air at inversion top. In this idealization, all the air in the CBL is given thermodynamic properties lying on these mixing lines. The thermodynamic profiles for clear and cloudy air within the CBL are modeled by giving different values to the parameter β in (3). For the clear-air (unsaturated) environment between clouds (solid lines in Fig. 6) we specified $\beta_u = 0.3, 1.2$, respectively, below cloud base and above cloud base (up to the inversion base), consistent with observations of the CBL structure over the oceans (Betts and Albrecht 1987; Betts and Boers 1990). The resolved inversion-layer thickness was fixed at two model layers (about 20 hPa), with a linear transition of p^* across it. For the cloud region profiles (short dashes), we specified $\beta_c = 0.2, 0.6$ respectively below cloud-base and in the cloud layer (up to the inversion base). The value of $\beta_c = 0.2$ gives a subcloud layer beneath clouds, which is slightly more well mixed than between clouds. Above cloud base, $\beta_c = 0.6$ gives a cloud-layer liquid water profile that is 40% (corresponding to $1 - \beta_c$) of the adiabatic value, as an approximation to the subadiabatic values typical of shallow cumulus clouds and stratocumulus (Warner 1970; Albrecht et al. 1990; Boers and Betts 1988). The inset on Fig. 6 shows this liquid water profile. Cloud liquid water is specified to fall to zero (where $p^* = p$) one model level (about 10 hPa) above the inversion base, so that a well-defined cloud top is given at the middle of the inversion, where the temperature T_{CT} at the cloud-top boundary can then be computed. This is used in the radiative code of the model, and it is the temperature that is equated to the satellite cloud-top temperature in (2). This temperature lies, as shown, on the mixing line at the cloud-top pressure (Betts 1982). Note that relative to other temperatures near cloud top, this evaporating cloud-top temperature can be a minimum, if the mixing line is more unstable than the moist adiabat. As Fig. 6 shows, this representation gives us idealized clear and cloudy profiles, with a nearly well-mixed subcloud layer, and a conditionally unstable cloud layer capped by an inversion. It can be regarded as an extension of the mixed-layer CBL to a partially mixed structure. The CBL model couples this mixing-line representation of clouds and their clear-air environment to a radiation code and calculates radiative–convective equilibrium solutions for the whole CBL structure given surface parameters: SST, surface wind speed, and surface transfer coefficient; free atmosphere parameters above the CBL; and cloud fraction. The radiation model has an elastic grid, with levels at cloud base and cloud top, and a vertical resolution within the CBL of about 10 hPa.

b. Input data for model equilibrium solutions

1) DATA USED

To simplify the presentation and clarify the simplifications inherent in the use of the model, we present an analysis of the changes with increasing SST along the northeast trade winds from near the California coast to 10°N for the 5-yr average July dataset. For the region in Fig. 2 east of the heavy streamline and south of 35°N, the data were binned into SST ranges of 1 K to give a mean profile with increasing SST of cloud-top temperature and fraction (from the satellite data) and surface pressure, air temperature, mixing ratio, and wind from the COADS data. From Figs. 1 and 7, it is clear that this flow is over uniformly increasing SST under relatively uniform overlying θ_{es}.

2) EQUILIBRIUM ASSUMPTION

Can a one-dimensional equilibrium model be of diagnostic value where the advection along the trajectory is over warmer water? Schubert et al. (1979a,b) and Albrecht (1984) in two-dimensional studies over the same region showed that the memory time for the thermodynamic properties of a well-mixed boundary is $\approx Z_I/(C_T V_0 + W_e)$ where Z_I is CBL depth, C_T a surface transfer coefficient, V_0 is the surface wind, and W_e is a CBL top entrainment rate. In the stratocumulus regime over cold water, this gives a time scale of order 21 h for $Z_I \approx 1000$ m, $C_T \approx 1.3 \times 10^{-3}$, $V_0 \approx 7$ m s^{-1}, $W_e \approx 0.4$ cm s^{-1}. However, our model does not have a well-mixed structure throughout the CBL, and probably a more relevant time scale for thermodynamic equilibrium of the subcloud layer is $Z_B/C_T V_0 \approx 15$ h for $Z_B \approx 500$ m. The SST gradient is ≈ 1 K (250 km^{-1}), so lag times of 15 h at 7 m s^{-1} would suggest sea–air temperature differences of ≈ 1.5 K, which is generally larger than appears in the COADS data (see Fig. 11). Probably the thermal lag of the sub-

cloud layer θ below the SST is reduced still further by the strong longwave radiative coupling with the surface. The net clear-sky radiative cooling in the subcloud layer is ≈ -2.5 K day^{-1} (greater at night and less in daytime) with larger values near the surface. This suggests that the radiative adjustment time of the subcloud layer with sea–air temperature differences of ≤ 1 K is of order half a day or less.

Schubert et al. (1979b) also showed that the equilibrium time for boundary-layer depth was much longer, comparable to the time scale of $1/D = Z_I/W_e$, where D is the mean divergence in the CBL, which decreases along the trajectories from 6×10^{-6} s^{-1} near the coast to 2×10^{-6} s^{-1} in the tropics (Schubert et al. 1979b; Bretherton 1990). This corresponds to adjustment times for CBL depth increasing from 2 to 5 days downstream. Thus, it is likely that the CBL will not have reached its equilibrium height, as it is advected over warmer water. However, our equilibrium model is not being used to predict equilibrium height, since the inversion-top subsidence field is unknown. The model will be used diagnostically to estimate subsidence from inversion-top height and temperature. Equilibrium inversion height is very sensitive to the subsidence rate (Betts and Ridgway 1989), so in our diagnostic use of the model along trajectories on which the BL has not yet reached equilibrium height, the mean subsidence rate may be slightly overestimated. Small errors in the subsidence have only a small impact on the internal CBL properties; so that, despite using an equilibrium model, the comparison with the deck-level COADS data is satisfactory. In fact it appears that over cold water, our estimates of the mean subsidence are too low (see section 3c).

3) SURFACE DATA

At the surface the equilibrium model needs the following as input: surface pressure p_0 and sea surface temperature SST and surface wind speed V_0 and drag coefficient, C_D, which are combined in the model in a surface transfer parameter $\omega_0 = \rho_0 g V_0 C_D$ (where ρ_0 is a surface air density). The model uses a fixed value of $C_D = 1.3 \times 10^{-3}$. Table 1 shows the distribution with SST of p_0, V_0, and ω_0 (calculated from the data). The COADS data also gives air potential temperature θ_A and mixing ratio q_A and the derived θ_{eA}: these will be compared with the equilibrium model solutions in section 3c.

4) CBL TOP DATA

At CBL top, we averaged (with respect to SST) θ_{es} and q from the NMC 700-hPa analyses shown in Figs. 7 and 8 to the southeast of the heavy streamline shown in Fig. 2. The data are shown in Table 1.

5) SATELLITE DATA

The satellite cloud fraction data given also in Table 1 are used as input to the CBL model, which calculates radiative fluxes for a clear and cloudy CBL. The cloud-top temperature data are matched by varying the model subsidence; this simultaneously gives the CBL top height.

6) SUMMARY OF MIXING-LINE RETRIEVAL

For completeness, Table 1 also lists cloud base and cloud top from the mixing-line retrieval in section 2. These will be compared with the equilibrium model solutions later. In addition, Table 1 includes Γ_{CBL}, the mean lapse rate from surface to cloud top derived from Fig. 10, and Γ_{ML}, the mixing-line slope through the cloud layer, normalized by the slope of the wet adiabat (subscript w)

$$\Gamma_{\mathrm{ML}} = (\delta\theta^*/\delta q^*)_{\mathrm{ML}}(\delta\theta/\delta q)_w^{-1}. \quad (4)$$

c. *Equilibrium model results*

The model equilibrium cloud-top temperature was matched to the satellite cloud-top temperature by varying the subsidence. Agreement was obtained to about ± 0.1 K. The COADS deck-level data were then

TABLE 1. Averages along mean trajectory toward increasing SST for COADS and satellite data and selected parameters derived from equilibrium CBL model.

Surface							CBL top		Satellite		Mixing-line retrieval			
SST (K)	P_O (hPa)	V_O (m s^{-1})	ω_O (Pa s^{-1})	θ_A (K)	q_A (g kg^{-1})	θ_{eA} (K)	θ_{es} (K)	q (g kg^{-1})	Cloud (%)	T_{CLD} (K)	P_T (hPa)	P_B (hPa)	Γ_{CBL} (K km^{-1})	Γ_{ML}
289.83	1017.0	7.73	.121	288.49	10.07	316.8	352.9	3.44	62.1	283.7	918.0	971.8	7.1	0.81
291.18	1018.1	7.54	.117	289.70	10.38	319.1	351.9	3.24	64.0	283.5	901.4	958.7	7.5	0.73
292.17	1018.5	7.18	.111	290.52	10.79	321.1	351.6	3.16	69.2	284.0	898.8	954.6	7.8	0.64
293.14	1017.6	6.72	.104	291.54	11.33	323.8	351.2	3.29	66.9	284.9	901.8	950.2	8.1	0.55
294.17	1017.4	6.51	.100	292.50	11.99	326.8	350.4	3.36	67.3	284.9	887.2	948.8	8.0	0.50
295.24	1016.7	6.44	.099	293.55	12.64	329.8	350.8	3.34	73.1	284.8	871.5	945.0	7.9	0.46
296.19	1015.8	6.81	.104	294.55	13.54	333.5	351.0	3.53	68.2	285.6	869.8	946.4	8.0	0.40
297.15	1015.0	6.92	.105	295.57	14.16	336.5	350.9	3.74	63.2	285.6	856.7	941.5	7.9	0.37
298.14	1014.8	7.46	.113	296.59	15.03	340.2	350.2	3.68	52.5	285.7	846.5	940.2	8.0	0.32
299.12	1013.3	7.43	.112	297.66	15.97	344.2	350.9	4.55	47.0	296.2	839.8	938.6	8.0	0.30
300.12	1012.1	7.00	.105	298.44	16.99	348.2	350.5	6.06	34.8	285.9	815.8	942.5	7.7	0.34
301.05	1011.5	5.40	.081	299.14	17.21	349.6	350.2	6.62	26.3	285.5	801.0	934.6	7.8	0.37

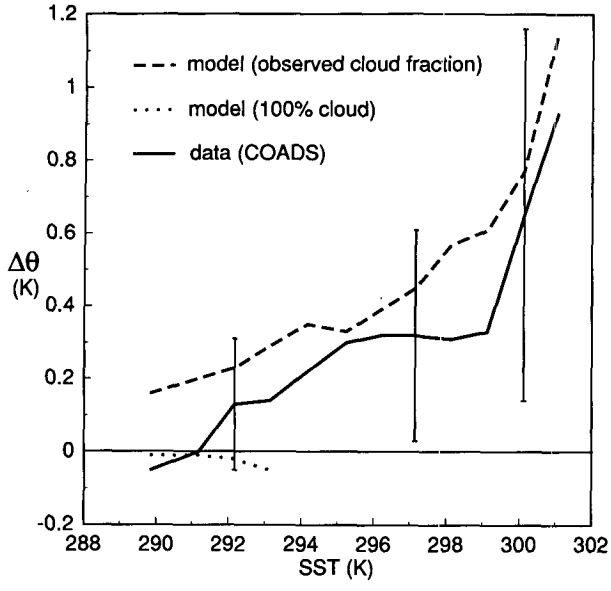

FIG. 11. Dependence of sea–air potential temperature difference $\Delta\theta$ on SST.

compared with the model solution as a test of the usefulness of the equilibrium solution.

1) COMPARISON WITH THE SURFACE COADS DATA

Figure 11 shows the sea–air difference $\Delta\theta$ for the mean COADS data (solid line) and the model solution (dashed) as functions of SST. The model solution has a slightly larger sea–air θ difference ($\approx$0.2 K) than the COADS data. Error bars indicate the large scatter in the COADS data, increasing with SST. Both data and model show a general increase of $\Delta\theta$ with SST. In the equilibrium model, the sea–air temperature difference increases with SST because cloud fraction, which controls the equilibrium longwave cooling of the subcloud layer, generally decreases. At cool temperatures, the model solution (dotted) is also shown for 100% cloud cover (with all other input conditions the same). When the cloud cover is 100%, the subcloud layer warms slightly and $\Delta\theta$ becomes small and negative in the model. This dotted solution is shown because the COADS data are long-term averages (five Julys) and cloud fraction is an average of both cloudy and cloud-free days, but the cloud-top temperatures are retrieved only for days with some cloud. At the coldest SSTs, where stratocumulus is common, there is a possibility that the cloud-top temperatures may be more representative of days having nearly 100% cloud cover.

Figure 12 shows the coupling between ship deck-level mixing ratio q_A and SST for the data (solid) and the model solution (dashed). The error bars indicate typical standard deviations of the data. The agreement is encouraging, but the model solution is more moist at both low and high SSTs by $\approx$0.4 g kg^{-1}. The dotted line at low SSTs is again the model solution corresponding to 100% cloud cover. A larger cloud fraction gives stronger CBL cooling, so a greater subsidence is needed to match the observed cloud-top temperature (and corresponding CBL depth). Thus, larger subsidence gives a lower equilibrium q_A. There is an indication again that the higher model values of q_A at low SSTs may be connected with too low a cloud fraction. One additional limitation of our analysis is that it is averaged over the diurnal cycle and the mean cloud fraction is greater at night than in the daytime.

Figure 13 shows θ_{es} at CBL top (which is the 700-hPa NMC analysis value) and the steep rise of low-level θ_{eA} with SST; the agreement is very similar to that in Fig. 12. Because θ_{es} above the CBL varies very little with SST along this mean streamline, there is a rapid decrease in mixing-line stability with increasing SST, until deep convection becomes likely at the warmest SSTs, as $\theta_{eA} \approx \theta_{es}$ (CBL top). Indeed, it is this deep convection that links the mean θ_{es} above the CBL to the low-level θ_{eA} over the high SSTs. Figures 11–13 suggest that the coupling between SST and the subcloud layer is so tight that despite the advection over warmer water, the thermodynamic properties of the near-surface air are quite close to the model equilibrium solutions ($\leq$0.2 K, $\leq$0.5 g kg^{-1}). This is extremely encouraging, since it suggests that simple equilibrium models can be used to reconstruct CBL structure over the oceans in data-void regions and perhaps improve estimates of the surface sensible and latent heat fluxes.

2) COMPARISON OF CLOUD BASE AND CLOUD TOP

Figure 14 shows the comparison of cloud-top (p_T) and cloud-base (p_B) pressure between data (solid) and model using the observed mean cloud-fraction data (dashed) and an assumed 100% cloud fraction at low

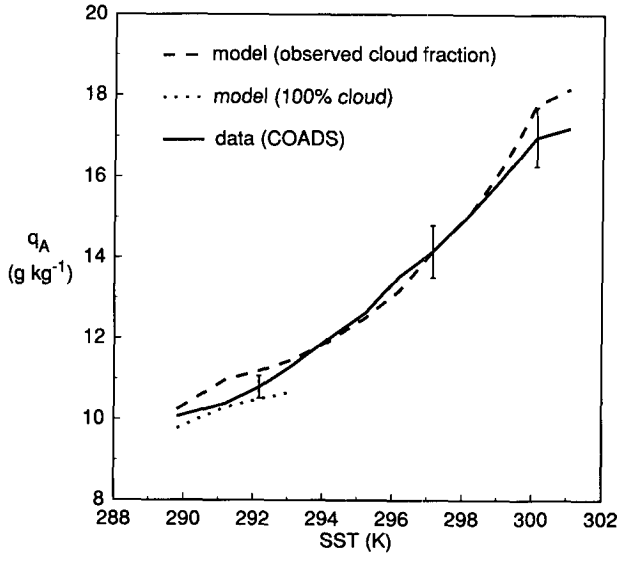

FIG. 12. Dependence of mixing ratio q_A at ship deck level on SST.

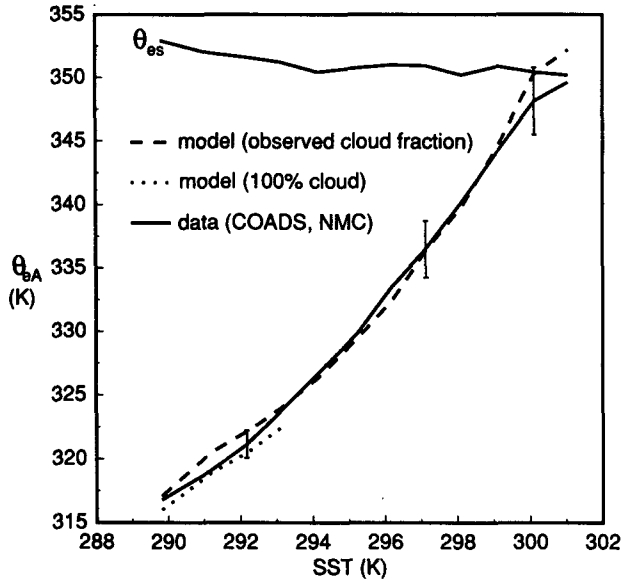

FIG. 13. As Fig. 12 for deck-level equivalent potential temperature θ_{eA} and saturated equivalent potential temperature θ_{es} above the CBL.

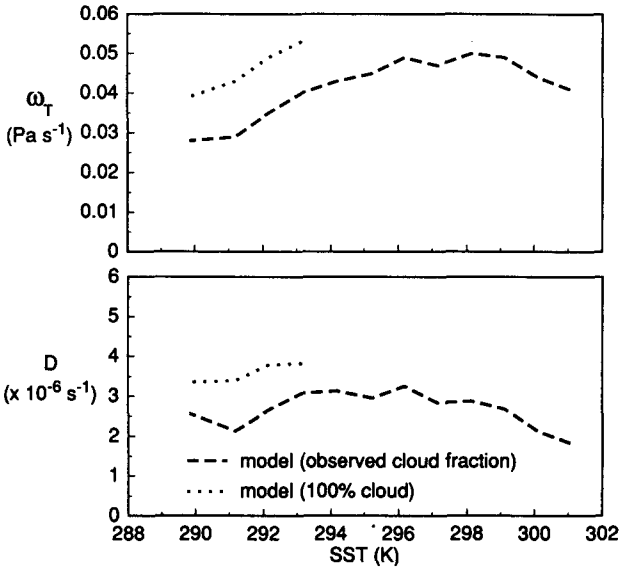

FIG. 15. As Fig. 12 for diagnosed subsidence parameter ω_T and horizontal divergence D.

SSTs (dotted). The agreement in cloud top is closely related to the matching of cloud-top temperatures. The differences at cloud base are related to the differences in near-surface θ_A and q_A seen in Figs. 11 and 12. We see that cloud-base pressure can be retrieved to about ±10 hPa using the equilibrium model.

3) DIAGNOSED SUBSIDENCE FIELD

The cloud-top temperature in the equilibrium model was matched to the satellite-observed cloud-top temperature by varying the CBL-top subsidence parameter ω_T in the model (Betts and Ridgway 1989). Figure 15 shows the variation of this diagnosed subsidence parameter with SST for the model solution (dashed), together with the mean CBL divergence D given by

$$D = -\delta\omega/\delta p = \omega_T(p_0 - p_I)^{-1}, \qquad (5)$$

where p_0 is the surface pressure, and $p_I = (p_T - 10)$ hPa is the inversion-top pressure. There is a smooth trend in diagnosed subsidence. The values at warm SSTs of $\omega_T \approx 0.045$ Pa s^{-1} and $D \approx 2.10^{-6}$ s^{-1} are consistent with those found in Betts and Ridgway (1988, 1989) for the deep tropics. At low SSTs, the diagnosed ω_T and divergence both decrease. The dotted curves are the higher values found if 100% cloud cover is assumed in the model. However, for SSTs below 293 K, even these values of the divergence of $\approx 3.5 \times 10^{-6}$ s^{-1} are low in comparison with Schubert et al. (1979b) and Bretherton (1990), who show values for the surface divergence in the range of 4–6 $\times 10^{-6}$ s^{-1} in this region. This discrepancy is unresolved. As discussed in section 3b, our equilibrium model ignores the mean horizontal advection in this region. In addition, the NMC and surface data in our five-July average include a wide range of conditions, both clear and cloudy, while the satellite cloud-top temperature data are limited to conditions of some boundary-layer clouds.

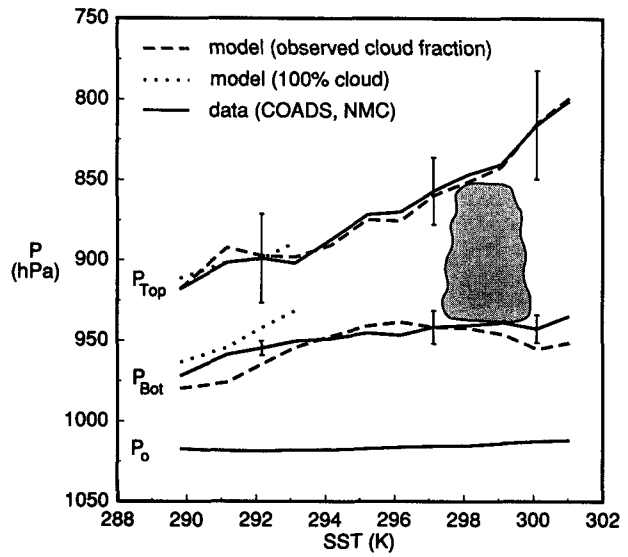

FIG. 14. As Fig. 12 for CBL-top pressure, cloud base, and surface pressure.

4. Conclusions

We have shown how a mixing-line model can be used to retrieve CBL depth from satellite cloud-top temperatures provided sufficient supporting data are available. To test the method, NMC data were used as an upper boundary condition, and the COADS surface

data averaged over five Julys (1983–1987) in the northeast Pacific were used at the surface. We found that the constant-lapse-rate method of retrieving CBL depth from SST and cloud-top temperature is quite satisfactory for the analysis region in the northeast Pacific, although the mean lapse rate through the CBL in most of this region is generally some 10% higher than the value of -7.1 K km^{-1}, proposed by Minnis et al. (1992) based on soundings near the coast.

Since atmospheric surface data are not always available over the oceans, we then explored the use of an equilibrium CBL model to give the CBL structure between the surface and inversion top. We matched the observed cloud-top temperatures by varying the mean subsidence and then compared the equilibrium model low-level potential temperature and mixing ratio with the COADS data; good agreement was found, to ≤ 0.2 K and ≤ 0.5 g kg^{-1}. This suggests that simple equilibrium models may have potential for improving the retrieval of detailed boundary-layer structure over the oceans, where limited data is available. Here we have combined a variety of different data sources, but one could envisage an iterative retrieval procedure using satellite data alone. Satellite temperature and moisture soundings have poor boundary-layer resolution but could give an estimate of (θ, q) above the CBL. These could be used together with satellite estimates of SST, surface wind speed, and boundary-layer cloud-top temperature and cloud fraction as boundary conditions for a radiative–convective CBL model. The boundary-layer profiles from the equilibrium model could be then reinserted into retrieval algorithms to derive improved temperature and moisture profiles in the lower troposphere.

Acknowledgments. A. K. Betts has been supported by the National Science Foundation under Grant ATM-9001960 and the NASA Goddard Space Flight Center under Contract NAS5-30524. We are grateful to Dan Cayan and Howard Hanson for the processed COADS data. The satellite analyses have been supported in part by the Office of Naval Research USN-N000149IMP24011.

REFERENCES

Albrecht, B. A., 1984: A model study of downstream variations of the thermodynamic structure of the trade winds. *Tellus,* **36A,** 187–202.

——, C. W. Fairall, D. W. Thompson, A. B. White, J. B. Snider, and W. H. Schubert, 1990: Surface based remote sensing of the observed and the adiabatic liquid water content of stratocumulus clouds. *Geophys. Rev. Letters,* **17,** 89–92.

Betts, A. K., 1973: Non-precipitating cumulus convection and its parameterization. *Quart. J. Roy. Meteor. Soc.,* **99,** 178–196.

——, 1982: Saturation point analysis of moist convective overturning. *J. Atmos. Sci.,* **39,** 1484–1505.

——, 1985: Mixing line analysis of clouds and cloudy boundary layers. *J. Atmos. Sci.,* **42,** 2751–2763.

——, and B. A. Albrecht, 1987: Conserved variable analysis of boundary layer thermodynamic structure over the tropical oceans. *J. Atmos. Sci.,* **44,** 83–99.

——, and W. Ridgway, 1988: Coupling of the radiative, convective and surface fluxes over the equatorial Pacific. *J. Atmos. Sci.,* **45,** 522–536.

——, and ——, 1989: Climatic equilibrium of the atmospheric convective boundary layer over a tropical ocean. *J. Atmos. Sci.,* **46,** 2621–2641.

——, and R. Boers, 1990: A cloudiness transition in a marine boundary layer. *J. Atmos. Sci.,* **47,** 1480–1497.

Boers, R., and A. K. Betts, 1988: Saturation point structure of marine stratocumulus clouds. *J. Atmos. Sci.,* **45,** 1157–1175.

Bretherton, C. S., 1990: Modelling the Lagrangian evolution of cloud-topped boundary layers. *Indo–U.S. Symp. on Parameterization in Global Models.* Pune, India, National Science Foundation and the India Institute of Tropical Meteorology, 15 pp.

Heck, P. W., B. J. Byars, D. F. Young, P. Minnis, and E. F. Harrison, 1990: A climatology of satellite-derived cloud properties over marine stratocumulus regions. *Conf. on Cloud Physics,* San Francisco, Amer. Meteor. Soc., J1–J7.

Kloessel, K. A., and B. A. Albrecht, 1989: Low level inversions over the tropical Pacific: Thermodynamic structure of the boundary layer and the above-inversion moisture structure. *Mon. Wea. Rev.,* **117,** 87–103.

Lilly, D. K., 1968: Models of cloud-topped mixed layers under a strong inversion. *Quart. J. Roy. Meteor. Soc.,* **94,** 292–309.

Minnis, P., and E. F. Harrison, 1984: Diurnal variability of regional cloud and clear-sky radiative parameters derived from GOES data. Part I: Analysis method. *J. Climate Appl. Meteor.,* **23,** 993–1011.

——, ——, and G. G. Gibson, 1987: Cloud cover over the equatorial eastern Pacific derived from July 1983 OSCCP data using a hybrid bispectral threshold method. *J. Geophys. Res.,* **92,** 4051–4073.

——, P. W. Heck, D. F. Young, C. W. Fairall, and J. B. Snider, 1992: Stratocumulus cloud properties derived from simultaneous satellite and island-based instrumentation during FIRE. *J. Appl. Meteor.,* **31,** 317–339.

Reynolds, R. W., 1988: Real-time global sea surface temperature analysis. *J. Climate,* **1,** 75–86.

Sadler, J. C., L. Oda, and B. J. Kilonsky, 1976: Pacific Ocean cloudiness from satellite observations. UHMET 76-01, 137 pp. [Available from the authors at the University of Hawaii, Honolulu.]

Schubert, W. H., J. S. Wakefield, E. J. Steiner, and S. K. Cox, 1979a: Marine stratocumulus convection. Part I: Governing equations and horizontally homogeneous solutions. *J. Atmos. Sci.,* **36,** 1286–1307.

——, ——, ——, and ——, 1979b: Marine stratocumulus convection. Part II: Horizontally inhomogeneous solutions. *J. Atmos. Sci.,* **36,** 1308–1324.

——, P. E. Ciesielski, T. B. McKee, J. D. Kleist, S. K. Cox, C. M. Johnson-Pasqua, and W. L. Smith, 1987: An analysis of boundary layer sounding data from the FIRE marine stratocumulus experiment. Atmospheric Science Paper No. 419, Department of Atmospheric Science, Colorado State University, Ft. Collins, 101pp.

Stull, R. B., 1973: Inversion rise model based on penetrative convection. *J. Atmos. Sci.,* **30,** 1092–1099.

Tennekes, H., 1973: A model for the dynamics of the inversion above a convective boundary layer. *J. Atmos. Sci.,* **30,** 558–567.

Timchalk, A., 1986: Satellite derived moisture profiles. NOAA Tech Rep. NESDIS 24, 60 pp. [Available from NTIS, U.S. Dept. of Commerce, Sills Bldg. 5285 Port Royal Rd., Springfield, VA 22161.]

Trenberth, K. E., and J. G. Olson, 1988: An evaluation and intercomparison of global analyses from the National Meteorological Center and the European Center for Medium Range Weather Forecasts. *Bull. Amer. Meteor. Soc.,* **69,** 1047–1057.

Warner, J., 1970: On steady-state one-dimensional models of cumulus convection. *J. Atmos. Sci.,* **27,** 1035–1040.

Woodruff, S. D., R. J. Slutz, R. L. Jenne, and R. M. Steurer, 1987: A comprehensive ocean–atmosphere data set. *Bull. Amer. Meteor. Soc.,* **68,** 1239–1250.